Article

Spatiotemporal Patterns Evolution of Residential Areas and Transportation Facilities Based on Multi-Source Data: A Case Study of Xi'an, China

Xinyi Lai [1] **and Chao Gao** [2],*

1   School of Architecture and Planning, Anhui Jianzhu University, Hefei 230601, China; xinyi@stu.ahjzu.edu.cn
2   College of Transportation Engineering, Chang'an University, Xi'an 710061, China
*   Correspondence: 2018023004@chd.edu.cn; Tel.: +86-182-0292-1671

Abstract: The spatiotemporal patterns of residential and supporting service facilities are critical to effective urban planning. However, with growing urban sprawl and congestion, the spatial distribution patterns and evolutionary characteristics of these areas show significant uncertainty. This research was conducted for six phases from 2012 to 2022, incorporating datasets of point of interest (POI) data for residential areas and transportation facilities (RATFs) and OpenStreetMap (OSM) data. Using exploratory spatial data analysis (ESDA) and standard deviation ellipse, we investigated the spatiotemporal patterns and directional characteristics of RATFs in Xi'an, as well as their evolution and underlying causes. The analysis demonstrated that: (1) The spatial distribution of RATFs in Xi'an exhibits non-uniform and gradually evolving patterns, with significant spatial agglomeration characteristics over the past decade. Residential areas (RAs) exhibit a spatial autocorrelation that is high in the middle and low in the surrounding areas, while transportation facilities (TFs) exhibit spatial patterns that are high in the southern and low in the northern areas. (2) Overall, the number of RATFs has continued to increase, and they exhibit significant spatial autocorrelation. Specifically, the trend of RAs concentrating in the central city has become increasingly prominent, while TFs have expanded from the center to the north. (3) Furthermore, from the perspective of supply–demand matching, this study proposes targeted adjustment strategies for the distribution of RATFs. It provides significant references for the optimization of service facilities and provides new ideas and practical experience for urban spatial analysis methods based on multi-source data.

Keywords: spatial autocorrelation; spatiotemporal patterns; standard deviation ellipse; point of interest; urban planning; Xi'an

1. Introduction

The rational and scientific layout of urban spaces serves as the foundation for urban expansion and development. The planned distribution of various functional areas in the city directly affects the vitality of urban development [1]. The spatial distribution and evolution of residential areas and transportation facilities (RATFs) are critical components of urban planning and development [2]. Residential areas (RAs) and transportation facilities (TFS), as two of the most basic urban spaces, have a profound impact on the quality of life [3,4], traffic conditions [5], and ecological environment of cities [6]. With cities continuing to expand and become more congested, it is essential to comprehend the spatiotemporal patterns and directional characteristics of RATFs to plan and optimize service facilities effectively [7]. Therefore, in-depth research on the spatiotemporal dynamics of RATFs can provide an important theoretical basis and practical experience for optimizing urban spatial structures [8,9].

Traditionally, socio-economic data, satellite images, and on-site observations have been used to study the distribution patterns of urban RATFs [10]. However, with the advent of big data technology, innovative approaches and technical tools have emerged,

making it a hot research topic in modern urban planning [11]. The increasing availability of multi-source big data has made electronic navigation maps based on point of interest (POI) and OpenStreetMap (OSM) data particularly useful in urban spatial planning [12]. These data cover every corner of modern cities and provide longitude, latitude, and other attribute information that is fast, simple, efficient, and low cost and has wide coverage [13]. Recently, the increasing availability of multi-source urban big data has provided new opportunities for exploring urban spatial structures and dynamics [14–16]. Studies have used POIs [13,17,18], social media [19,20], mobile phone data [21], and remote sensing images [20,22,23] to identify urban functional areas, analyze population distribution, evaluate public facilities, and understand travel behaviors. They can help identify urban functional areas and play a groundbreaking role in comprehensive and detailed urban development planning [19].

There are some potential shortcomings of the current research in this field: (1) Lack of integrated analysis. Most studies focused on a single data source, such as POIs, social media, mobile phone data, or remote sensing images. Limited research has integrated multiple data sources to obtain a comprehensive understanding of urban spaces. Our study aims to fuse POIs, OSM data, and other sources to explore the spatiotemporal dynamics of RATFs. (2) Coarse resolution. Many studies were conducted at a coarse resolution, such as the city level or district level. High-resolution analysis at the street block or building level is still limited. Our research will examine the evolution of RATFs at a high resolution (high level of detail). (3) Static analysis. Although some studies have analyzed urban dynamics, most research has explored urban spatial structures at a single time point [24]. Systematic analysis of the spatiotemporal evolution and trends of urban spaces is still lacking. Our research aims to investigate how RATFs have evolved from 2012 to 2022. (4) Lack of comparative analysis. Few studies have compared the spatial distribution and dynamics across different cities. Cross-city comparative analysis can provide additional insights into the drivers and mechanisms shaping urban spaces. Our research focuses on a case study of Xi'an, and comparative analysis with other cities is limited. (5) Limited application. Most studies stayed at an exploratory level, with limited applied values in urban planning and management. Translating research findings into targeted policy recommendations and solutions that can optimize urban spatial structures is needed. Our study aims to provide recommendations for adjusting the allocation of RATFs in Xi'an. (6) Lack of integrated modeling. Although some studies have used land use simulation models, integrated modeling that incorporates multiple data sources is still lacking. Developing data-driven models that can simulate future changes of urban spaces will provide useful tools for urban planning. Our research has not involved modeling, which can be improved in future studies.

In summary, future research can focus on fusing multi-source data, conducting high-resolution and spatiotemporal analysis, enabling cross-city comparative studies, providing applicable policy recommendations, and developing integrated simulation models. These can help gain a more comprehensive understanding of urban dynamics and provide effective support for smart city planning [25]. Therefore, a comprehensive analysis of the spatiotemporal patterns of these areas and facilities is essential for informed decision making in urban planning and development [26]. To achieve this goal, this paper aims to use multi-source data to investigate the spatiotemporal patterns of residential areas and transportation facilities in Xi'an, China. The study will employ various methods, including the standard deviation ellipse and point of interest analysis, to explore the distribution and correlation of features in the urban environment. The results of this study will provide valuable insights into the spatiotemporal patterns of Xi'an's residential areas and transportation facilities and will be of great significance for the city's urban planning and development.

This study aims to explore the spatiotemporal patterns and evolution of residential areas and transportation facilities (RATFs) in Xi'an, China, from 2012 to 2022 using point of interest (POI) data and OpenStreetMap (OSM) data. Specifically, we examine the distri-

bution characteristics, spatial autocorrelation, directional trends, and underlying drivers of RATFs' evolution. The results can provide targeted recommendations for adjusting the allocation of urban service facilities and optimize the spatial structure of Xi'an.

The rest of the paper is organized as follows: Section 2 describes the study area and methods. Section 3 shows the results of the spatiotemporal patterns of RATFs in Xi'an by year. Section 4 provides a discussion of analysis results. Finally, Sections 5 and 6 summarize the paper and provide suggestions for future research.

2. Materials and Methods

2.1. Study Area

Xi'an, the capital of Shaanxi province in central-western China, is considered one of China's leading tourist destinations and is well regarded for its international image. This paper focuses on a portion of Xi'an's main urban area, specifically the districts of Lianhu, Weiyang, Xincheng, Beilin, Yanta, Baqiao, and some townships in Chang'an District, covering an area of approximately 729.1 square kilometers, as shown in Figure 1.
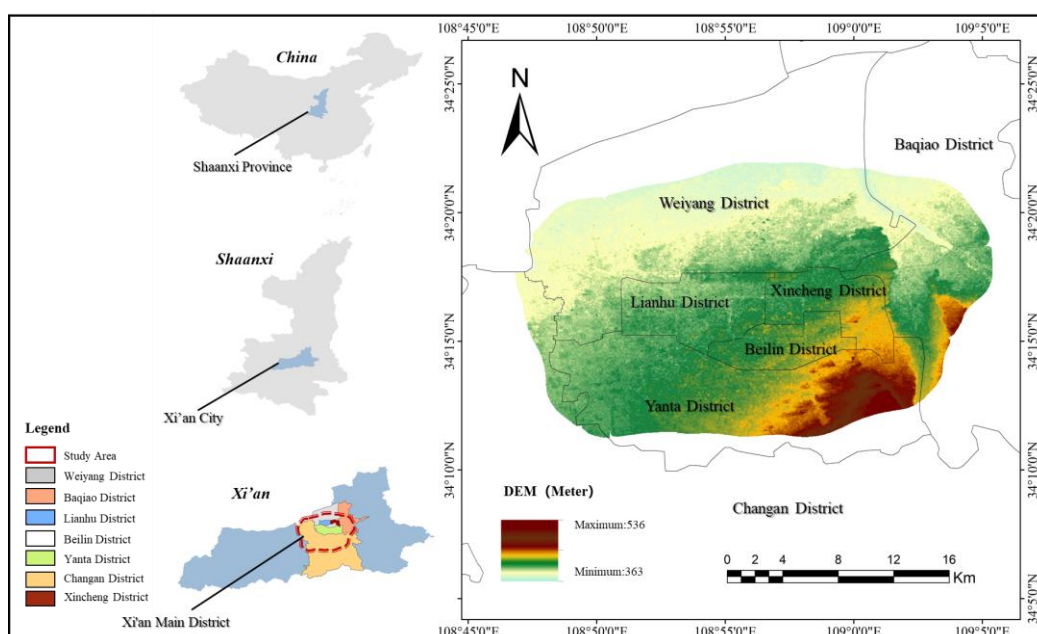

Figure 1. Study area.

Seven districts constitute Xi'an's main urban area, with a total population of nearly 10 million in 2022. These districts have distinctive development priorities under the official city's master plan. Specifically, Lianhu District aims to develop its commercial and residential sectors while preserving historical heritage. It has a population of 1.2 million. Weiyang District, with a population of 1.5 million, focuses on high-tech industrial parks and emerging industries. Xincheng District seeks to become a modern financial and commercial center through urban renewal. It is home to a population of 1.1 million. Beilin District prioritizes cultural preservation and tourism, especially around its heritage sites. Its population is 0.9 million. Yanta District plans to build itself into an education and research hub, with a population of 1.3 million. Baqiao District strives to lead in modern agriculture and ecology. It has a population of 1 million. The selected townships in Chang'an District, with a population of about 1.2 million, aim for balanced development of scientific and technological innovation and humanistic ecology.

We selected Xi'an as the study area due to its unique as well as typical characteristics that signify its importance for investigating the spatiotemporal dynamics of RATFs. In 2022, Xi'an's permanent population exceeded 10 million, cementing its status as a super metropolis in western China. Currently, the Chinese government is devoted to developing new urban centers and promoting balanced, sustainable regional growth. An in-depth

spatiotemporal study of the evolution of infrastructure in Xi'an can generate important insights for these national development strategies. In summary, its dense population, flat terrain, and stable administration provide integrated data to track the city's development over space and time. Xi'an offers an informative case study for sustainable city building and infrastructure improvement.

2.2. Datasets

The study investigated Xi'an's main urban area, utilizing Crawling API technology to extract POI data from Baidu Maps, an open geospatial platform. Since its launch in 2011, Baidu Maps' open platform data and classification standards have been continuously improved to better apply POI data to research on urban built environments. Furthermore, referencing Baidu POI tags (http://lbsyun.baidu.com/index.php?title=open/poitags, accessed on 22 June 2022), POI data classification for RATFs was selected, as shown in Table 1. The category of TFs includes subway stations, bus stations, train stations, parking lots, and long-distance bus stations. The RAs category includes residential neighborhoods, villa districts, industrial parks, dormitories, community centers, office buildings, and mixed-use buildings. POI data has 19 tags, including basic information such as name, category, address, and coordinates. It is valuable in the spatial analysis of public facilities due to its easy accessibility, wide coverage, and vast sample size [27]. Furthermore, these geographical entities are closely related to people's daily lives.

Table 1. POI data classification for RATFs from Baidu POI tags.

	Residential Areas (RAs)	Transportation Facilities (TFs)
POI Classification	Villas, industrial parks, industrial and related buildings, business office buildings, commercial and related residential, commercial and residential dual-use buildings, community centers, dormitories, residential areas	Taxi, subway station, service area, port terminal, bus station, railway station, airport-related buildings, warning information, toll station, parking lot, long-distance bus station

Prior to classifying the POI data, we conducted data cleaning and coordinate conversion. This involved removing duplicate, erroneous, null, and spatiotemporally offset records to ensure data accuracy and completeness. Ultimately, 98% of the data were retained, with a total of 1,462,606 POIs across the six time periods. Finally, to further reduce the impact of overall POI growth on infrastructure, this study primarily employed the proportional data of facilities to more accurately capture the laws of spatial evolution in cities. This study has revealed the changing trends for RAs and TFs in the main urban area of Xi'an over the past decade (2012–2022), as shown in Table 2.

Table 2. The amount, proportion, and changing trend of RATFs' POI data by years.

Years	Total POI of RATFs	Number of RAs POI	Proportion of RAs	Changing Trend	Number of TFs POI	Proportion of TFs	Changing Trend
2012	72,809	6250	8.58%	/	2990	4.11%	/
2014	113,747	9223	8.11%	↓	4968	4.37%	↑
2016	263,786	12,167	4.61%	↓	9100	3.45%	↓
2018	291,821	15,786	5.41%	↑	14,800	5.07%	↑
2020	293,131	11,147	3.80%	↓	14,947	5.10%	↑
2022	354,322	8855	2.50%	↓	14,579	4.11%	↓

In 2012, the supply of TFs in Xi'an had not yet saturated. Over the past decade, Xi'an continuously expanded its TFs, resulting in marked improvements to the transportation network, as shown in Figure 2. The number of TFs rose from 2990 in 2012 to 14,579 in 2022. RAs exhibited a comparable growth trend, signifying increased provision of functional service facilities overall in Xi'an. However, analyzing the total RATFs revealed

more complex dynamics. From 2012 to 2016, RATFs experienced rapid growth, indicating substantial infrastructure development. Yet, in 2018, growth rates for both RAs and TFs slowed, suggesting diminishing demand. Then, from 2020 to 2022, despite a resurgence in total RATFs, the proportions of RAs and TFs declined sharply. This signifies a shift not merely in the scale but also in the aims and purposes of infrastructure expansion in Xi'an over the study period. While accumulation continued, the societal needs and functions being served evolved. Decelerating growth followed by surging totals alongside declining proportions points to revolutions in infrastructure demand and provision over the decade.
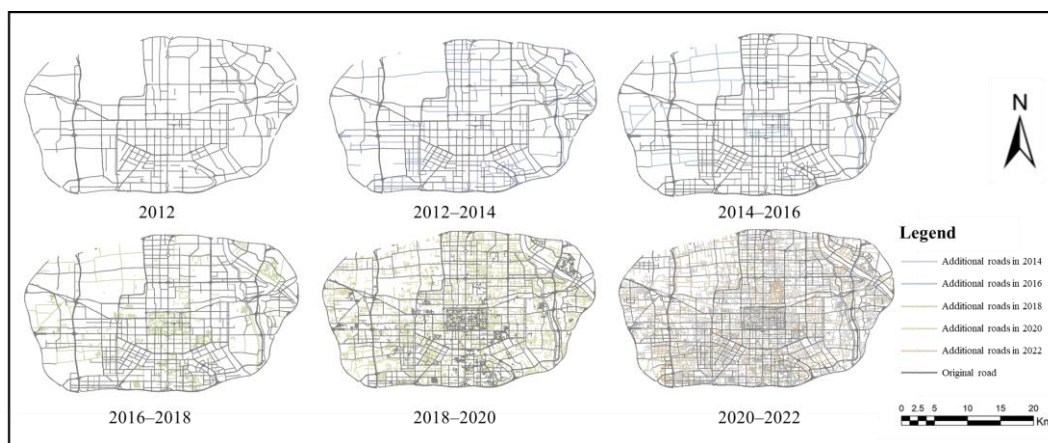
Figure 2. OSM road network data.

The road network data for Xi'an were obtained from Open Street Map (http://download.geofabrik.de/asia.html, accessed on 22 June 2022). The OSM road network data possess advantageous qualities such as high timeliness, strong operability, and high resolution [28]. In order to further improve the quality of the data, this study has utilized methods such as manual visual interpretation and on-site surveys to extract road network data of various levels within each research area, serving as the fundamental data for subsequent research.

Figure 2 illustrates the distribution of three types of OSM roads (trunk, primary, and secondary) in 2012, with the additional roads becoming increasingly dense every two years as time progresses. Serving as crucial transportation infrastructure, road network data offer insights into the dynamics of TFs. Similarly, the evolution of the roads positively influences the aggregation and development of the road network. OSM data provide valuable insights for our analysis, helping us understand the spatial context of RATFs.

2.3. Methods

2.3.1. Research Framework

Traffic analysis zones (TAZs) are small geographic units used for transportation planning and travel demand analysis, representing zones of relatively homogeneous travel behavior and socioeconomic characteristics. In this study, the TAZs were designated by the Xi'an Traffic Committee, and we further refined them based on the distribution of POI data combined with the DBSCAN algorithm [29]. Within the main urban area of Xi'an, we ultimately identified 202 TAZs, covering a range of 0.76–4.93 square kilometers. These TAZs enabled a finer-grained investigation of infrastructure dynamics across Xi'an's urban space. In addition, the basic geographic dataset used in this paper includes spatial analysis data containing Xi'an POI RATFs data and OSM data from 2012–2022. The study employs various methods including kernel density analysis, ESDA, and standard deviation ellipse to derive spatiotemporal patterns of the evolution of Xi'an from 2012 to 2022. Based on this, a comparison of six phases is conducted, and the underlying causes affecting the spatiotemporal patterns of RAs and TFs in Xi'an are analyzed. Finally, the paper summarizes

the evolution of spatiotemporal patterns and provides solutions. The research framework is shown in Figure 3.
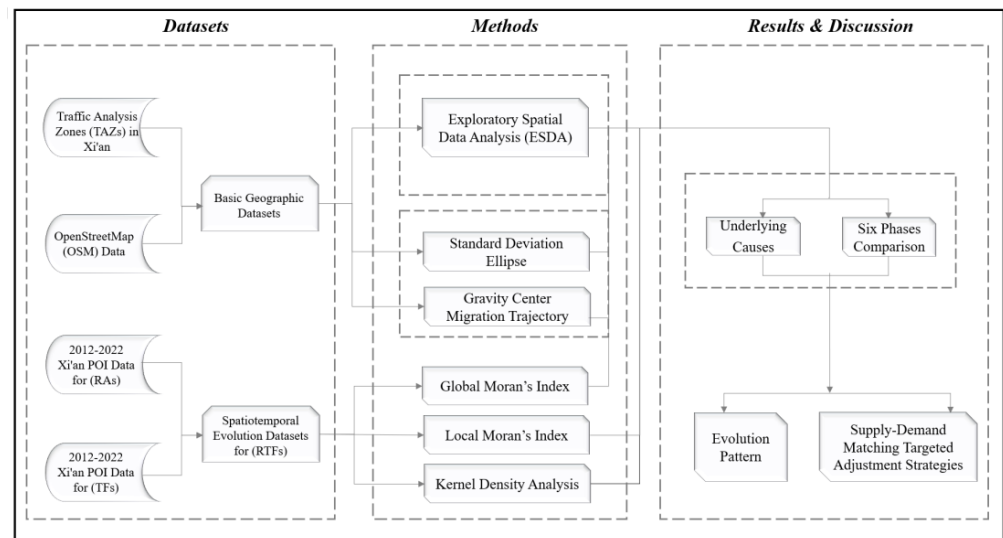
Figure 3. Research framework.

Kernel density analysis and exploratory spatial data analysis have been widely used in spatial research to understand and visualize spatial patterns and relationships. Kernel density analysis allows for the estimation of continuous spatial patterns from discrete point data [30], making it suitable for analyzing the distribution of RATFs in our study area. Similarly, exploratory spatial data analysis provides a range of techniques for understanding spatial autocorrelation and identifying clusters and hotspots within the data [31]. Previous studies have employed these methods to successfully investigate various spatial phenomena, such as urban land use, transportation networks, and environmental factors.

While using a single method may provide some insights into spatial patterns, it may also introduce potential biases, inaccuracies, and uncertainties associated with the data and methods, as well as any assumptions made during the analysis. By combining multiple methods, such as kernel density analysis and exploratory spatial data analysis, our study benefits from a more robust and nuanced understanding of the spatiotemporal patterns of RATFs.

2.3.2. Kernel Density Analysis

Kernel density analysis is a method that uses kernel functions to calculate the density of the surrounding area of a point feature [32]. By entering the overall features, the degree of aggregation of the point features within the entire study area can be calculated, thus forming a continuous density surface on a plane. In this study, this method was employed to identify the aggregated RAs' and TFs' distribution in Xi'an. The kernel density formula is represented in Equation (1):

$$P_i = \frac{1}{n\pi R^2} \times \sum_{j}^{n} K_j \left(1 - \frac{D_{ij}^2}{R^2} \right)^2 \tag{1}$$

In the equation, P_i represents the kernel density of the i facility point in the study area; R denotes the selected bandwidth of the rule area; K function represents the spatial weight function; D_{ij} indicates the distance between facility point i and research object j ($D_{ij} < R$, when D_{ij} reaches a certain value, $R = 0$); and n represents the number of research objects R within the bandwidth j range.

2.3.3. Exploratory Spatial Data Analysis

Exploratory spatial data analysis (ESDA) is a commonly used research methodology to characterize spatial distribution, distinguish spatial correlation features, and identify spatial outliers. In empirical analysis, two spatial data analysis methods, global spatial autocorrelation and local spatial autocorrelation, are frequently utilized to measure and examine spatial distribution patterns [33].

The global spatial autocorrelation is the overall spatial distribution patterns and aggregation effect of measured objects, reflecting their spatial dependence. The Global Moran's Index is commonly used to measure it. The formula for calculating the Global Moran's Index is as follows:

$$I = \frac{\sum_{i=1}^{n} \sum_{j=1}^{n} w_{ij}(x_i - \overline{x})(x_j - \overline{x})}{S^2 \sum_{i=1}^{n} \sum_{j=1}^{n} w_{ij}} \tag{2}$$

where $S^2 = \frac{\sum_{i=1}^{n}(x_i - \overline{x})^2}{n}$ represents the sample variance, and w_{ij} represents the spatial weight matrix. If TAZs i and j share common boundaries or vertices, $w_{ij} = 1$ holds true, otherwise $w_{ij} = 0$ denotes the sum of all spatial weight matrices. The range of Moran's I generally lies within $[-1, 1]$. Values greater than 0 indicate a positive correlation, less than 0 indicate a negative correlation, and equal to 0 indicate no correlation.

The local spatial autocorrelation primarily reflects the local variability and correlation degree of the elements, indicating their spatial heterogeneity. The Local Moran's Index is commonly used to measure it. The formula is as follows:

$$I_i = \frac{(x_i - \overline{x})}{S^2} \sum_{j=1}^{n} w_{ij}(x_i - \overline{x}) \tag{3}$$

The Local Moran Index formula conveys a similar meaning to that of the Global Moran Index. Here, $I_i > 0$ represents the enclosure of high values surrounding TAZs i or low values surrounding it, while $I_i < 0$ represents the enclosing of a low value in TAZs i by high values or vice versa. If the number of RAs or TFs in TAZs i is similar to that of the neighbors, the TAZs exhibit patterns of high-high or low-low aggregation.

2.3.4. Standard Deviation Ellipse

This study uses the standard deviation ellipse analysis method to investigate the spatial distribution and orientation of point features and utilizes the centroid migration trajectory model to reveal their spatiotemporal pattern evolution [34]. This method comprehensively displays the spatial arrangement and evolution characteristics of point features by calculating parameters such as azimuth, major and minor axes, and central point. The formula for calculating the centroid, X and Y semi-axes, and azimuth angle of the ellipse is represented in Equation (4):

$$\begin{cases} \overline{X} = \sum_{i=1}^{n} X_i W_i \Big/ \sum_{i=1}^{n} W_i \\ \overline{Y} = \sum_{i=1}^{n} Y_i W_i \Big/ \sum_{i=1}^{n} W_i \end{cases} \tag{4}$$

The coordinates of the standard ellipse centroids, $\overline{X}$ and $\overline{Y}$, are given in Equation (5). The coordinates of pixels i are denoted by X_i and Y_i, while W_i represents the weight and n the total number of pixel elements.

$$\tan\theta = \frac{\sum_{i=1}^{n} \overline{X}_i^2 W_i^2 - \sum_{i=1}^{n} \overline{Y}_i^2 W_i^2 + \sqrt{\left(\sum_{i=1}^{n} \overline{X}_i^2 W_i^2 - \sum_{i=1}^{n} \overline{Y}_i^2 W_i^2\right)^2 + 4\left(\sum_{i=1}^{n} \overline{XY} W_i\right)^2}}{2 \sum_{i=1}^{n} \overline{XY} W_i}$$

$$\begin{cases} \sigma_x = \frac{\sqrt{2 \sum_{i=1}^{n} \left(\overline{X}_i W_i \cos\theta - \overline{X}_i W_i \sin\theta\right)^2}}{n} \\ \sigma_y = \frac{\sqrt{2 \sum_{i=1}^{n} \left(\overline{Y}_i W_i \sin\theta + \overline{Y}_i W_i \cos\theta\right)^2}}{n} \end{cases} \tag{5}$$

In the given formula, σ_x and σ_y respectively denote the standard deviation along the X and Y axes, that is, the lengths of the X and Y axes, while n represents the total number of pixels.

3. Results

3.1. Kernel Density Distribution for RATFs

Using the kernel density tool in ArcGIS software, an analysis of RATFs in Xi'an was conducted for six phases between 2012 and 2022 [35]. The kernel density analysis was performed to detect hotspots and the clustering of RAs and TFs over time. The kernel density analysis identified the absolute hotspots of RATFS, revealing clustered areas with the highest density for each infrastructure type over the study period. Examining the spatiotemporal changes in these hotspot areas facilitated exploration of the dynamics and relationship between residential and transportation development across Xi'an's urban space from 2012 to 2022, as shown in Figures 4 and 5.
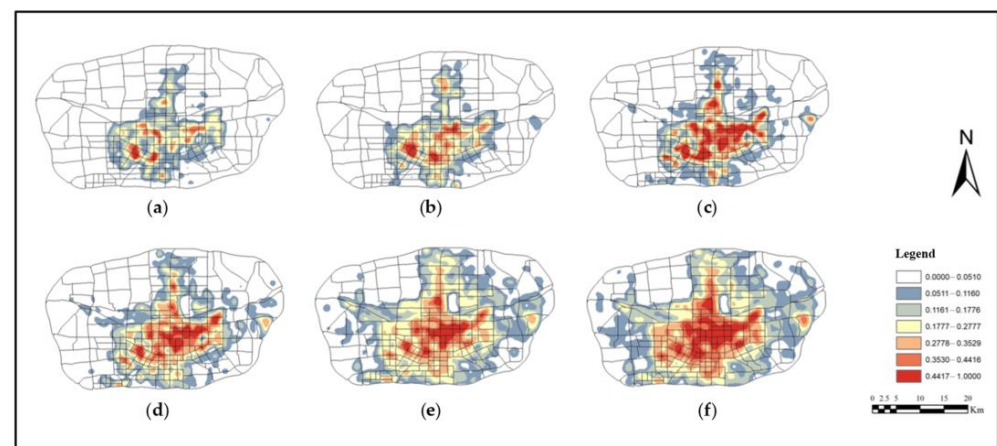
Figure 4. Six phases' kernel density of RAs in Xi'an: (**a**) 2012 RAs; (**b**) 2012–2014 RAs; (**c**) 2014–2016 RAs; (**d**) 2016–2018 RAs; (**e**) 2018–2020 RAs; (**f**) 2020–2022 RAs.
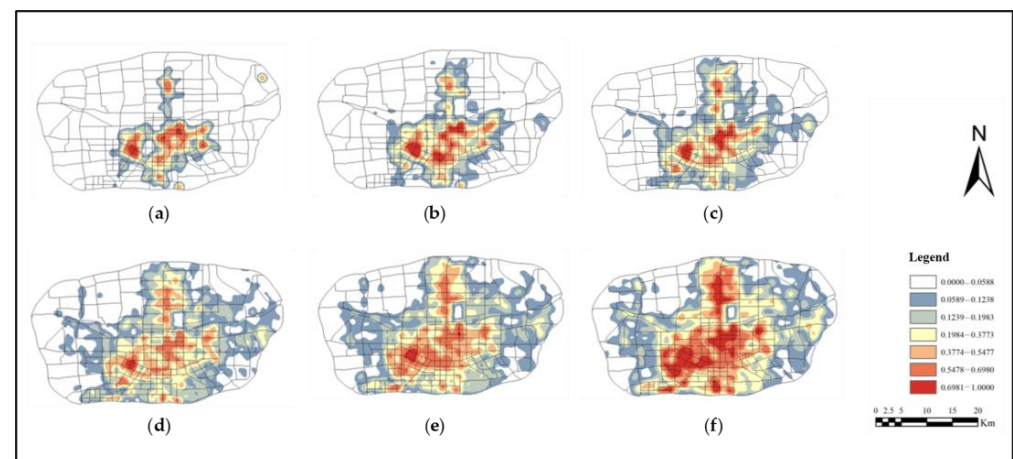
Figure 5. Six phase kernel density analysis of TFs in Xi'an: (**a**) 2012 TFs; (**b**) 2012–2014 TFs; (**c**) 2014–2016 TFs; (**d**) 2016–2018 TFs; (**e**) 2018–2020 TFs; (**f**) 2020–2022 TFs.

3.1.1. Analysis of Kernel Density Distribution for RAs

The kernel density distribution of RAs in Xi'an from 2012 to 2022 exhibits distinct spatial regularity characteristics, as shown in Figure 4. Xi'an's main urban area had already reached the aggregated distribution status in RAs in 2012, and the degree of aggregation has been increasing year by year. By 2022, the distribution of TFs in Xi'an's main urban area exhibited a typical "core–periphery" structure. The "core area" is mainly distributed

within Xi'an's inner ring road and tends to extend towards the western outer ring road. The "core area" has a stable ring structure, with the first ring being particularly stable and the second ring showing a tendency to extend to the northwest. Only around the second ring of the core area, there is an irregular circular aggregation forming the third ring, which then constitutes a three-ring hierarchical structure within the inner part of the outer ring road. The "sub-core area" outside the outer ring road presents typical dotted patterns and is highly dependent on radial arterial roads. The spatial distribution patterns of the "sub-core area" are diverse. The "sub-core area" only surrounds the core area in an irregular circular shape within the inner ring road and its vicinity and has not formed an independent dotted aggregation. The TFs density sub-core area consists of an irregular circular area tightly surrounding the core area and a scattered dotted area on the periphery. The spatial form of the scattered dotted area has high stability and is almost entirely located in the center of each district.

It can be inferred from the figure that there is a significant aggregation of RAs in the inner circle (0–1 km) of each transport station area, and the degree of aggregation is significant. Among them, the RAs in the area where Xi'an Station is located have the most extensive aggregation center. Apart from the inner circle, several obvious high-density areas also appear in the outer circle (2–3 km), while the kernel density value in the middle circle (1–2 km) is generally low. As for the RAs in the aggregation center of Xi'an North Station, there are multiple high-density points scattered across each circle, and the number of high-density points is significant.

3.1.2. Analysis of Kernel Density Distribution for TFs

With the help of the ArcGIS kernel density tool, a visual analysis of the spatial distribution characteristics of TFs in Xi'an was carried out and is depicted in Figure 5. Higher kernel density values indicate denser facility point distributions. It can be observed that the spatial layout of TFs in Xi'an has formed its own unique characteristics, exhibiting agglomerated distribution patterns with more facilities densely distributed in the central area and fewer facilities scattered on the periphery, showing the characteristic of being densely distributed in the south and sparsely distributed in the north. Specifically, in terms of aggregation, TFs in Xi'an's main urban area exhibit significant multi-centered distribution patterns. As the center city, the intersection of Lianhu District, Beilin District, and Xincheng District forms a high-density area, where TFs are distributed in a contiguous and aggregated manner with a noticeable aggregation effect. However, there are relatively high-kernel-density areas in the peripheral districts, but the aggregation effect is not significant, and the distribution of TFs is relatively small in scale and more dispersed.

Regional agglomeration is characterized by large agglomerations with scattered voids, presenting a spatial form of coexistence of diffusion and agglomeration. In areas far from the city center, the kernel density of TFs in Xi'an presents a spatial form characteristic of "aggregation and diffusion". In areas far from the center of Xi'an, TFs' kernel density shows a spatial form of "large aggregation and small diffusion"; the diffusion of TFs' kernel density mainly presents a spatial feature of continuous large-scale diffusion.

Overall, high-density RAs and TFs in Xi'an have appeared in a large area of the junction of Beilin District, Lianhu District, and Xincheng District and have gradually dispersed to the surrounding areas, with a high degree of spatial overlap in their density distribution. The central connecting area is the old city area, which was the first area to develop in Xi'an. Various service facilities have undergone a long period of accumulation, and the population density is high. The level of economic vitality is at the forefront of the city, and the degree of transportation convenience is also relatively high, making it the main area for the distribution of various living service facilities. In addition to the old city area, RATFs in other districts have formed high-density agglomeration areas of varying scales in university towns, industrial parks, and comprehensive business districts, indicating that cultural environment, economic atmosphere, and other factors have a significant impact on the distribution of living service facilities in Xi'an. In addition, the development of RAs

lags behind that of TFs, and their main aggregation areas are also within the range of high density of other facilities.

3.2. Spatiotemporal Evolutionary Patterns for RATFs

3.2.1. Analysis of Spatiotemporal Evolutionary Patterns of RAs

The results of the global autocorrelation analysis indicate that from 2012 to 2022, the Global Moran's I Index for both RAs and TFs in Xi'an were positive, and their *p*-values were less than 0.05, as shown in Figure 6. It can be inferred that during this period, the distribution of RATFs in the TAZs of Xi'an's main urban area was not random. Moreover, the Global Moran's I Index for RAs in Xi'an was consistently greater than 0 from 2012 to 2022, and for most years, *p*-values were below 0.05, indicating that there was a significant spatial aggregation effect for RAs in Xi'an for most years.
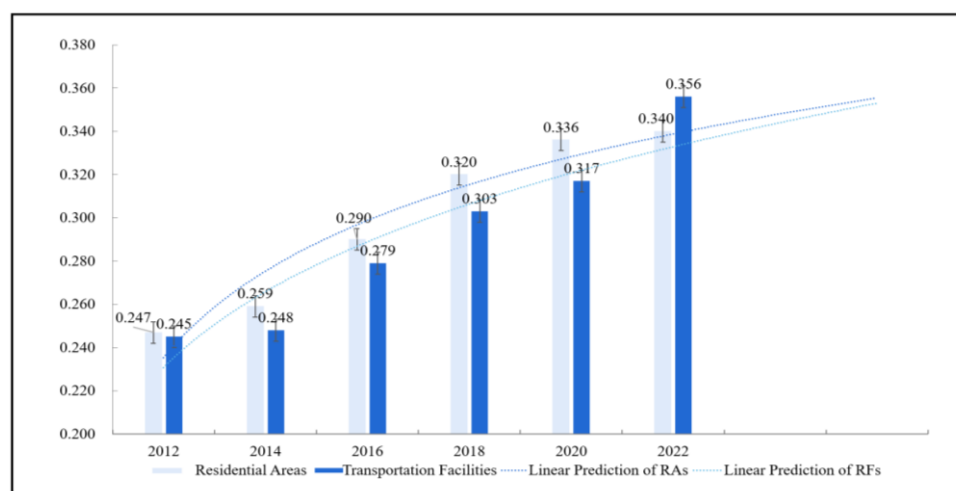

Figure 6. Global Moran Index evolution of RATFs in Xi'an by years.

High-high aggregation: As shown in Figure 7, from 2012 to 2022, the highly aggregated RAs in Xi'an have shifted as a whole towards the central and northern parts of the city. In 2012, the main highly aggregated area was located in Beilin District, while by 2022 it had expanded to include Beilin, Xincheng, and Lianhu districts. The areas with the high-high aggregation of RAs have high-density living services and wide service coverage, with high levels of transportation infrastructure and accessibility. These areas belong to the traditional core of the city, and from 2012 to 2022, the high-high aggregation areas included various historical sites such as Hanchang'an City Weiyang Palace National Archaeological Park, Daming Palace National Heritage Park, Tang Paradise, Shaanxi History Museum, Big Wild Goose Pagoda, and Xi'an Bell Tower, which have formed Xi'an's cultural and tourism core area. In addition, large commercial districts such as Zhongda International Business Center, World Window Technology Creative Industry Park, Starlight CityMore Shopping Center, Wanda Plaza, Zhongmao Plaza, Xi'an SKP, and Xi'an New World Fashion Square have formed hotspots for gathering facilities, including dining, shopping, leisure, and entertainment, thus forming the main commercial center of Xi'an's core area. Moreover, the Xi'an North Station, Xi'an Station, and Lianhu Station areas serve as the most important transportation hubs connecting to the outside of the main urban area.

Low-low aggregation: From 2012 to 2022, areas with low-low aggregation of RAs continued to expand. In 2012, only certain areas of Xi'an's Weiyang and Yan'ta districts exhibited such low-low aggregation. By 2022, low-low-aggregation areas had expanded to include parts of Weiyang, Yan'ta, and Baqiao districts. Overall, the trend of low-low-aggregation RAs expanding outward has continued. Regarding the low-low aggregation of RAs, overall, these areas exhibit a low-low aggregation of life service facilities, relatively poor life service functionality, and skewed transportation accessibility, and they are considered to be expanding areas at the edge of the inner circle. As urbanization accelerates and

local areas experience economic and population agglomeration and growth, the agglomeration of facilities gradually becomes more diverse. In multiple years from 2012 to 2022, the low-low aggregation included Xi'an Hengpu International Science and Technology Park, Xi'an Software New Town Software R&D Base, Xi'an National Digital Publishing Base, Huawei Xi'an Research Institute, China Xi'an Power System Co. Ltd., Shaanxi Surui New Material Co. Ltd., Schneider Electric Equipment Engineering Co., as well as Cainiao Xi'an Logistics Park, Shaanxi Digital Medicine Industrial Park, Fengdong Daming Palace Innovation Port, Fengdong Chuangzhi Yungu, and Wanwei Xi'an Fengdong Park, located in Weiyang District.
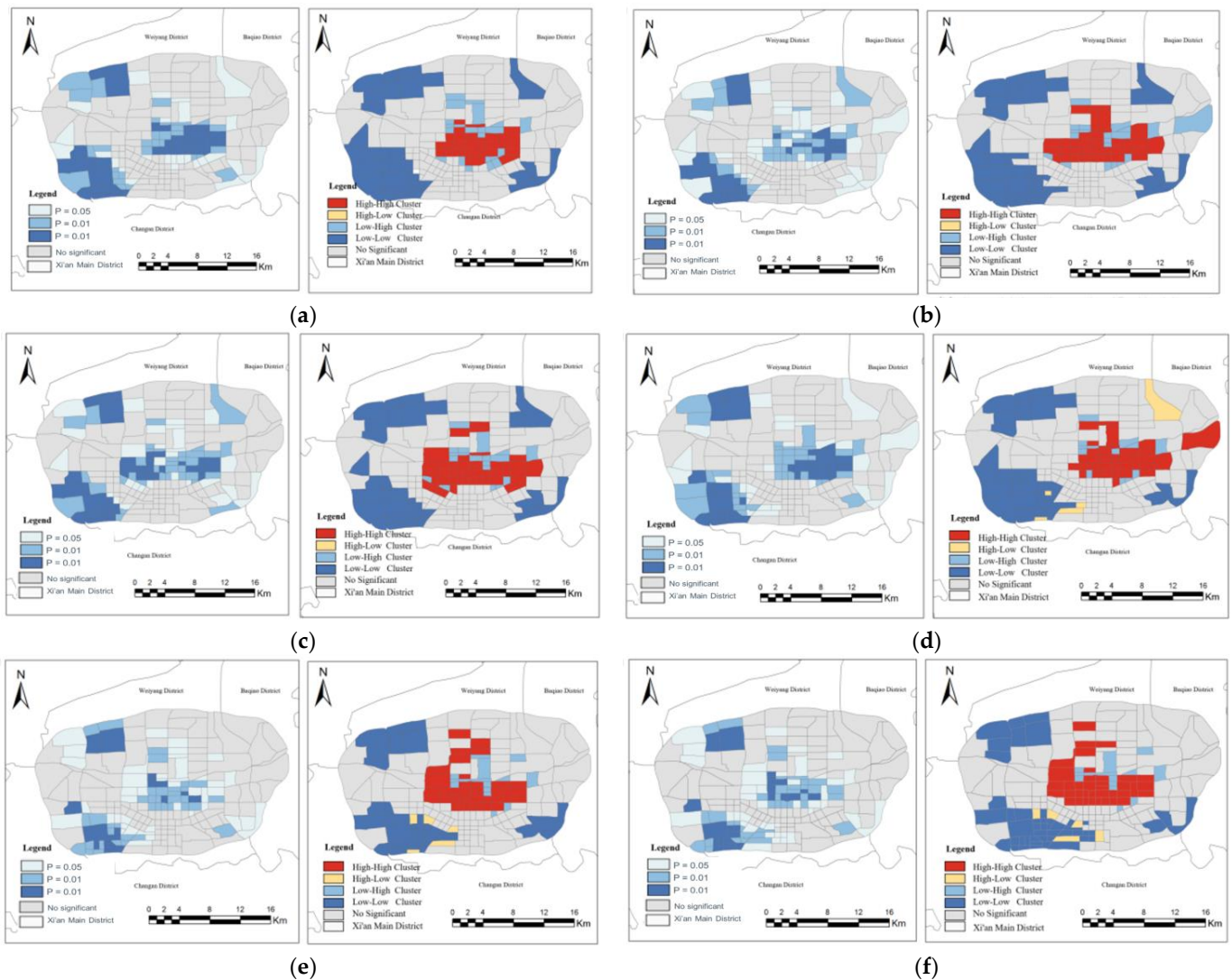
Figure 7. Six phases' local spatial autocorrelation patterns of RAs in Xi'an: (**a**) 2012 RAs; (**b**) 2012–2014 RAs; (**c**) 2014–2016 RAs; (**d**) 2016–2018 RAs; (**e**) 2018–2020 RAs; (**f**) 2020–2022 RAs.

High-low aggregation and low-high aggregation: From 2012 to 2022, there were few years and regions in Xi'an where RAs presented either high-low aggregation or low-high aggregation. These areas are mainly concentrated in the southwest of Weiyang District and the northwest of Yanta District. Most of them are industrial parks and lack residential and support living service facilities. In addition, they lack basic service infrastructure and are unable to meet the diverse needs of community residents. It is necessary to focus on diversifying the community, supporting living service facilities in these areas, and improving the convenience of life service facilities [36].

3.2.2. Analysis of Spatiotemporal Evolutionary Patterns of TFs

From 2012 to 2022, the Global Moran's Index of TFs in Xi'an passed a significance test with a significance level of 0.05. The Moran index was greater than 0, indicating a positive spatial correlation in the TFs of Xi'an's main urban area. Units with more TFs exhibited a phenomenon of spatial aggregation. As shown in Figure 6, the spatial autocorrelation of TFs has been increasing year by year since 2012, indicating that the spatial aggregation of TFs has been getting stronger. During this period, the fluctuations were stable, and Xi'an's main urban area experienced relatively stable spatial aggregation.

High-high aggregation: As shown in Figure 8, from 2012 to 2022, in Xi'an, aggregated TFs gradually expanded or shifted to surrounding regions. Initially, in 2012, the high-high aggregation area was mainly in the Beilin district of Xi'an's main urban area. However, by 2022, it included Yan'ta District, Weiyang District, and Xincheng District. The aggregated TFs of the regions as a whole have shifted to the north of Xi'an. Over the years from 2012 to 2022, the high-high aggregation of TFs area includes but is not limited to: Xi'an North Bus Station in Weiyang District, Xi'an City Hall, Daming Palace Subway Station, Hanyuan Temple Subway Station, Lianhu Train Station, Administrative Center Subway Station, Xi'an City Sports Park Cultural Center Square, and other areas. In addition, it includes the Dayan Pagoda subway station, Datang Furong Garden, Xi'an Qujiangchi Ruins Park, Xiaozhai subway station, Chang'an University, Xi'an University of Science and Technology, Shaanxi Normal University, and other areas in Yan'ta District.

These areas have a high-high aggregation of pedestrian traffic, well-connected road networks, and a dense public transport network, resulting in high traffic intensity and severe traffic congestion issues, as well as severe overloading of TFs. Therefore, it is suggested that TFs' operation bottlenecks be improved by correctly identifying the types of bottlenecks and controlling the traffic saturation of bottleneck sections. In addition, optimizing transport routes, prioritizing rapid transit on congested sections of transit routes, and paying attention to the locations of hub stations and bay-style transit stations should be considered to reduce the impact of bus traffic on road traffic flow. Improving the locations of transport stations, focusing on the connection between transport modes and transit conditions, and prioritizing public transit road rights are also important measures to consider. In addition, during peak travel times, when passenger and commuter traffic increases significantly, the pressure on transportation operations will be high, and some transportation routes may become excessively saturated. Therefore, it is recommended to increase the frequency of some buses during peak hours and to implement cross-station or fast/slow transit modes to reduce station stops. Finally, open streets where pedestrians and vehicles coexist are common, but pose serious traffic safety risks. Therefore, it is recommended to focus on inspection and prevention measures, and to implement corrective action for areas with high safety hazards and serious traffic violations.

Low-low aggregation: From 2012 to 2022, areas with low-low aggregation of TFs continued to expand. In 2012, only certain areas in Weiyang and Yanta districts were classified as having low-low aggregation of such facilities. However, by 2022, areas such as Weiyang, Yanta, and Baqiao districts were included in this category. Overall, low-low-aggregation transportation areas continued to expand outward from their centers. Over the years from 2012 to 2022, the low-low aggregation of TFs included the urban roads of Jianzhang Road, Fengye Avenue, Fengyue Road, Sun Wu Road, Feng'an Road, Fengquan Road, and Tianzhang 1st Road in the Weiyang district, as well as the urban roads of Keji 6th Road, Keji 8th Road, Hualong 2nd Road, Tangu 8th Road, Yunshui 1st Road, Jinye Road, Yunshui 3rd Road, and Tangu 9th Road in the Yanta district. These roads mainly connect to industrial parks and are located on the outskirts of Xi'an's inner ring road expansion area. In these areas, road density is low, connectivity is poor, bus service is infrequent, and the accessibility of the urban road network is inadequate. It is recommended to develop shuttle bus operations based on the characteristics of urban residents' travel needs, in order to improve the "last mile" connection problem and increase the coverage of transportation network services.
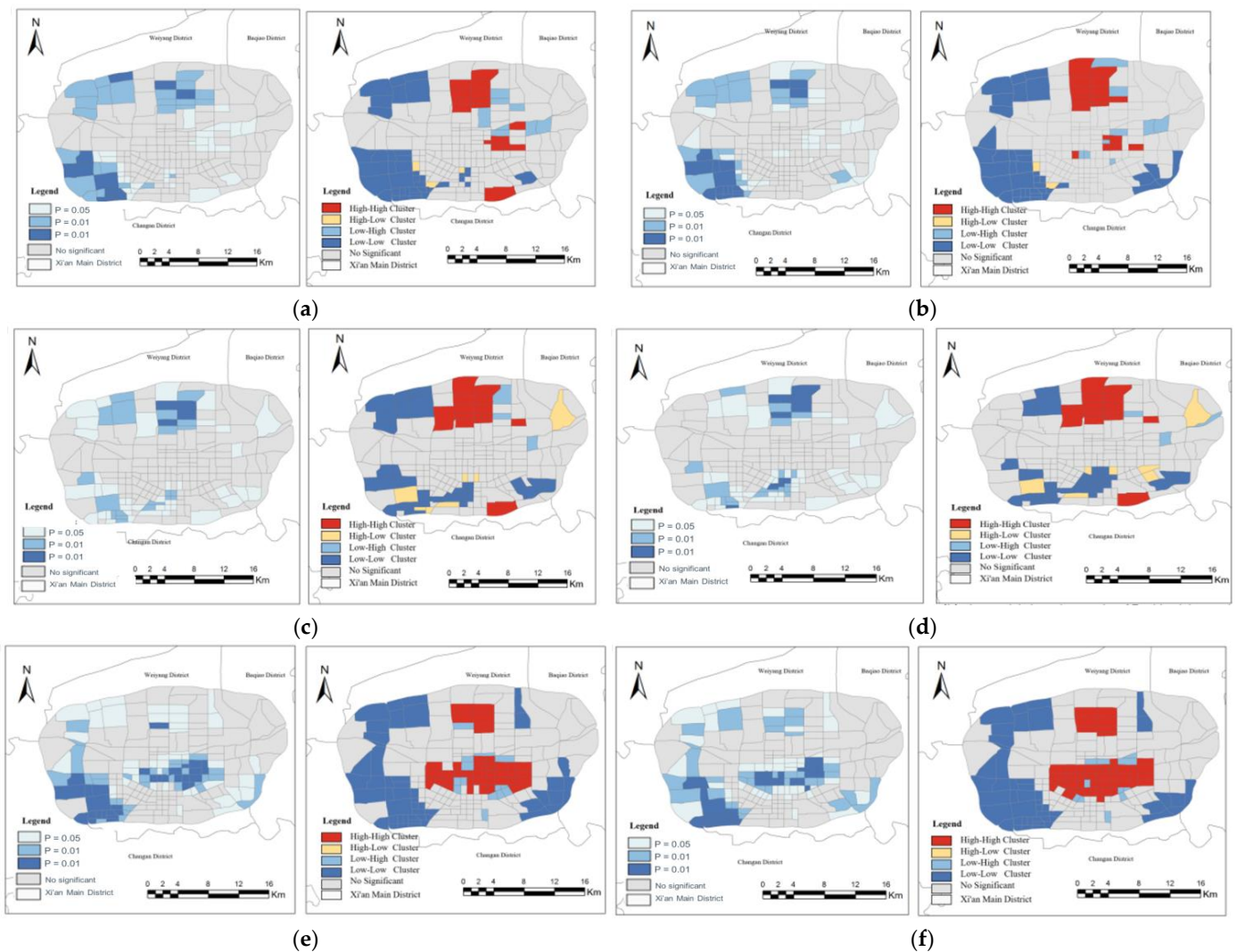
Figure 8. Six phases' local spatial autocorrelation patterns of TFs in Xi'an: (**a**) 2012 TFs; (**b**) 2012–2014 TFs; (**c**) 2014–2016 TFs; (**d**) 2016–2018 TFs; (**e**) 2018–2020 TFs; (**f**) 2020–2022 TFs.

High-low aggregation and low-high aggregation: From 2012 to 2022, there were relatively few years and regions in Xi'an where TFs exhibited either high-low or low-high aggregation. The main areas of high-high aggregation were surrounded by residential and service areas exhibiting either high-low or low-high aggregation, especially in Yan Ta, Xin Cheng, and Lian Hu districts. These areas are mainly located in old, antiquated urban districts adjacent to more economically robust primary commercial centers. Numerous residential complexes are constructed in close proximity to these commercial districts. These areas have clear land-use functions and a substantial scale of life-service facilities, which contributes to their high population densities. Therefore, the intensity of demand for residents' travel needs is significant. However, the level of supply of transport infrastructure is inadequate. Therefore, it is recommended to improve the convenience of residents' travel in this area by strengthening the construction of basic infrastructure and corresponding supporting service facilities, improving the construction of TFs within each community, increasing the accessibility and serviceability of stations, and expanding the coverage of the public transport network.

Using the single-quantity spatial autocorrelation univariate Local Moran's Index method, we calculated the Local Moran's Index for RAs and TFs between 2012 and 2022. Our results (Table 3) show that Moran's Index for RAs in Xi'an's main urban area increased from 0.2474 in 2012 to 0.3396 in 2022, suggesting a continuous strengthening of spatial

autocorrelation for RAs over the past decade. Similarly, the trend of change in Moran's I for TFs in Xi'an between 2012 and 2022 was similar to that of RAs. Although there were some differences in spatial layout over time, Moran's I for TFs increased from 0.2453 in 2012 to 0.3559 in 2022, indicating a continued strengthening of spatial autocorrelation for TFs over the past decade.

**Table 3.** Local Moran's Index of RAs and TFs by years.

Years	RAs			TFs		
	Moran's I	Z-Value	*p*-Value	Moran's I	Z-Value	*p*-Value
2012	0.2474	7.6457	0.001	0.2453	7.8657	0.001
2014	0.2594	8.0715	0.001	0.2481	8.0614	0.001
2016	0.2897	9.061	0.001	0.2787	8.5066	0.001
2018	0.3198	9.9722	0.001	0.3027	9.3436	0.001
2020	0.3359	10.4391	0.001	0.317	9.8991	0.001
2022	0.3396	10.7299	0.001	0.3559	11.1504	0.001

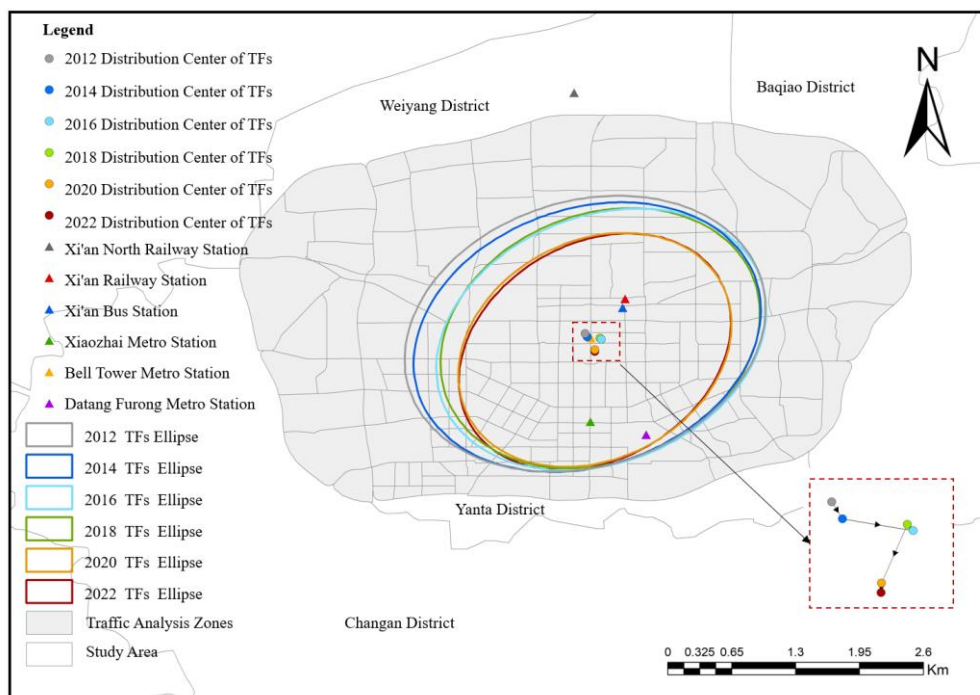*3.3. Gravity Center Migration Trajectory for RATFs*

This study employed the standard deviation ellipse analysis tool and the central analysis method in ArcGIS software to investigate the spatial distribution of RAs and TFs in Xi'an's main urban area from 2012 to 2022, as shown in Figures 9 and 10. The selected ellipse standard deviation level parameter is the default first level, covering 68% of the POI data points of RATFs in the study area. The research results show that the spatial distribution direction and center point of RAs and TFs in Xi'an have not changed significantly during this period. During this time, the center of gravity of the standard deviation ellipse of RAs in Xi'an has moved from (34°15′54″ N, 108°56′24″ E) to the southeast direction of (34°15′25.2″ N, 108°56′34.8″ E), as shown in Figure 8. At the same time, the center of gravity of the standard deviation ellipse of TFs in Xi'an has moved from (34°15′54″ N, 108°56′24″ E) to the southeast direction of (34°15′25.2″ N, 108°56′38.4″ E), as shown in Figure 6. The detailed areas where the centers of gravity are located will be explained in detail later in the paper. During this period, Xi'an actively promoted the construction of subway lines and continuously improved the transportation network in the main urban area.

3.3.1. Migration Trajectory of Gravity Center of RAs

Prior to 2012, RAs were primarily aggregated in the old and dilapidated urban areas of Xi'an, such as Xi'an Vehicle Factory Living Quarters, Xi'an Huayuan RAs, Xi'an Diaqiao RAs, and Xi'an Qujiang Wahu Tong RAs. However, with the opening of Xi'an's first subway line in September 2011, a total of eight subway lines with a total operating length of 279 km and 176 stations were opened in Xi'an by 2022, boosting its RAs. From 2012 to 2022, Xi'an Subway Line 2 traversed the main urban area of Xi'an from north to south, connecting important historical sites such as Xi'an Bell Tower, Xi'an City Wall, and Yongning Gate, with RAs such as Vanke Golden Field Huafu, Seville Community, Changshi Community, Bihai Community, and Mingdu City Community along the line. Along the route of Xi'an Subway Line 3, new RAs such as Bayi Community, Qindi Laclare Mansion, Taibai Community, Zhongtian International Apartment, Xinkexinyuan Garden Community, Postal Community, Yamei Building, Shangri-La Hotel, and Fengyun Blue Bay Community have been established. Xi'an Subway Line 4 runs through key tourist attractions such as Xi'an City Government, Hanyuan Hall, Heping Gate, Big Wild Goose Pagoda, Tang Paradise, and Dong Chang'an Street, attracting a large number of tourists to stay in the area. RAs along Xi'an Subway Line 4 include Kerry Center, Taihua Road Community, Xi'an Railway Daming Palace Community, Guanghua Community, Xi'an Sunshine International Hotel, Wanda Plaza, Furongge Hotel, and Furongfang Hotel.
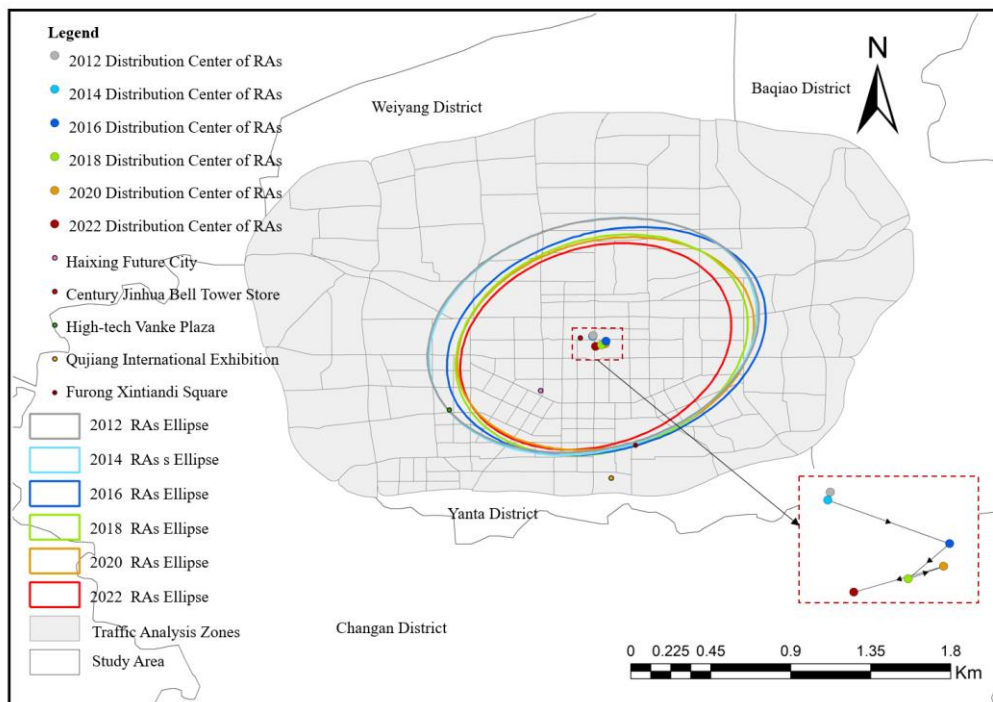
Figure 9. Gravity center and ellipse migration trajectory of RAs by years.

Figure 10. Gravity center and ellipse migration trajectory of TFs by years.

The central concept conveyed in Figures 9 and 10 are the relative spatial distribution of geographic elements in a two-dimensional plane, with azimuth reflecting the predominant trend in their distribution. The long axis serves as an indicator of the level of dispersion of geographic elements along the main trend direction, while the short axis represents the range of data distribution. As the short axis decreases in length, the centripetal force of the data becomes more pronounced. Oblateness is defined as the ratio of long and short axes and serves as an indicator of the degree of directionality of the data. A higher oblateness

value indicates a higher level of directional orientation in the data, while a lower oblateness value implies a greater degree of data dispersion.

According to Figure 9 and Table 4, the focus of RAs in 2022 has shifted to the southwest compared to 2012. Between 2012 and 2022, the main axis of the RAs in the northeast-southwest direction was shortened from 1.5577 km to 1.2849 km. This indicates a decrease in the dispersion of RAs in the northeast-southwest direction in the main urban area of Xi'an, and it also indicates that RAs are increasingly aggregated in the northeast-southwest direction. During the same period, the minor axis of RAs in the northwest-southeast direction decreased from 1.0516 km to 0.9151 km, indicating that the distribution range of RAs is becoming more aggregated and that the centripetal force of RAs development in 2022 is stronger. The flattening ratio decreased from 1.4813 to 1.4041 between 2012 and 2022. It can be seen that the ellipticity of 2022 is smaller than that of 2012, indicating that the directionality of RAs development in 2022 is weaker than that in 2012.

Table 4. Standard deviation ellipse results evolution of RAs by years.

Years	Center X	Center Y	Long Axis Length (km)	Short Axis Length (km)	Rotation	Oblateness
2012	108.9415	34.2623	1.5577	1.0516	76.4991°	1.4813
2014	108.9405	34.2619	1.5435	1.0602	75.4578°	1.4559
2016	108.947	34.259	1.5088	1.0064	73.7832°	1.4992
2018	108.9455	34.2579	1.3804	0.983	73.3093°	1.4043
2020	108.9473	34.2586	1.3941	0.9558	76.3314°	1.4586
2022	108.9427	34.2573	1.2849	0.9151	72.1454°	1.4041

3.3.2. Migration Trajectory of Gravity Center of TFs

Between 2012 and 2022, ellipses representing RAs and TFs showed a consistent contraction, indicating a close spatial relationship between the two, as shown in Figures 9 and 10. Furthermore, both RAs and TFs converged around the central area of Xi'an city, and compared to 2012, the major and minor axes of RATFs in the main urban area of Xi'an city were larger in 2022. This also suggests that the coverage and dispersion of RAs and TFs were more extensive in spatial distribution in 2022, as shown in Figures 6 and 7. Over the period from 2012 to 2022, with the continuous improvement of the Xi'an subway network, the subway and elevated bridges have made urban transportation more convenient, driving the continuous increase in RATFs in the surrounding areas of Xi'an's main urban area. In addition, Xi'an has many historical sites and cultural relics of significant historical value, such as the ruins of the Qin Dynasty Palace, the Big and Small Wild Goose Pagodas, Xi'an City Wall, the site of Mingde Gate, and Xi'an Bell Tower, which have attracted a large number of tourists to visit.

According to Figure 9 and Table 5, the center of gravity of TFs in 2022 shifted to the southwest compared to 2012. Between 2012 and 2022, the major axis of TFs in the northeast-southwest direction decreased from 1.6992 km to 1.3296 km. This indicates that the dispersion of TFs in the main urban area of Xi'an in the northeast-southwest direction has decreased, while the aggregation of TFs in the northeast-southwest direction has increased. During the same period, the TFs minor axis in the northwest-southeast direction decreased from 1.2228 km to 0.9948 km, indicating that the TFs distribution range has become more aggregated, demonstrating that the centripetal force of TFs development in 2022 is stronger. The flattening ratio fell from 1.3896 to 1.3366 between 2012 and 2022. It can be seen that the ellipticity of TFs in 2022 is smaller than that in 2012, indicating that the directional development of TFs in 2022 is weaker than that in 2012.

Table 5. Standard deviation ellipse results evolution of TFs by years.

Years	Center X	Center Y	Long Axis Length (km)	Short Axis Length (km)	Rotation	Oblateness
2012	108.9396	34.2649	1.6992	1.2228	72.9190°	1.3896
2014	108.9405	34.2633	1.6417	1.1855	71.1649°	1.3848
2016	108.9470	34.2622	1.5726	1.1357	68.3243°	1.3847
2018	108.9465	34.2628	1.5165	1.1419	68.6196°	1.3280
2020	108.9441	34.2575	1.3174	1.0063	62.9465°	1.3092
2022	108.9441	34.2566	1.3296	0.9948	59.8954°	1.3366

4. Discussion

Spatial autocorrelation, based on the first law of geography, highlights the impact of distance on the spatial distribution of phenomena. The spatial aggregation patterns of regional RAs are influenced not only by natural factors, such as altitude, terrain, and climate, but also by socio-economic factors such as surrounding operators, industry policies, market demands, and economic benefits. Previous research conducted at various levels (national, regional, and provincial) has demonstrated that spatial patterns of urban RAs exhibit aggregated, contiguous, or negatively correlated spatial patterns. It provides a scientific basis for the development and optimization of urban RATFs.

In this study, we analyzed the spatiotemporal patterns of RATFs in Xi'an's main urban area, using a comparative analysis model over several years and assessed the spatiotemporal patterns of RATFs from a multi-dimensional data perspective. RAs and TFs are essential living needs for urban residents, and with a large population in Xi'an, these services are increasing year by year to meet market demands. From the perspective of the Global Moran's Index, the positive role of spatial correlation has continued to strengthen, indicating an increasing degree of spatial aggregation and forming of core regions for RAs and TFs. It also provides a decision-making basis for optimizing the layout of these services.

Our analysis revealed that RAs exhibited positive spatial autocorrelation patterns overall. Over the past decade, the number of RAs in Xi'an's main urban area has undergone a process of initial decline, subsequent increase, and final decline, with the overall quantity continuing to increase. Global autocorrelation analysis indicated a positive spatial correlation between the number of RAs in Xi'an from 2012 to 2022. Concurrently, the number of TFs experienced a process of initial increase, subsequent decrease, subsequent increase, and final decrease, while the overall quantity has continued to increase. Global autocorrelation analysis results for TFs demonstrated a positive spatial correlation between the number of TFs in Xi'an's main urban area over the past decade. There are clear aggregation patterns in RATFs in Xi'an, and the degree of aggregation has continued to increase over time.

Our study found that RAs in Xi'an's main urban area have gradually formed agglomeration areas and established a core area for RAs. Local spatial autocorrelation analysis of RAs from 2012 to 2022 revealed high-high aggregation patterns in the central region of Xi'an, with a gradual shift towards the northern regions. Under the influence of RAs development, spatially uncorrelated states such as high-low aggregation and low-high aggregation have gradually evolved into spatially correlated patterns, such as high-high aggregation and low-low aggregation. Meanwhile, local spatial autocorrelation analysis showed that TFs in the central and northern regions of Xi'an exhibit high-high aggregation patterns and are increasingly aggregating towards surrounding areas.

5. Conclusions

This study focuses on the spatiotemporal patterns of RATFs in Xi'an's main urban area from the perspective of TAZs. The research reveals that the evolution of the spatiotemporal patterns of RAs and TFs in Xi'an can be divided into four stages: embryonic (prior to 2012), development (2012–2018), fluctuation (2019–2022), and recovery (2022–present). During these stages, the number of RAs and TFs has gradually increased, and their spatial distribution range has expanded. The center of gravity of RAs shifted from Beilin District

to Weiyang, Lianhu, and New City Districts due to the impact of the epidemic and then showed a trend of southwest migration during the recovery period.

Global Moran's Index and local spatial autocorrelation analysis indicate that the degree of aggregation of RAs and TFs has become more prominent over time. After the stabilization of the COVID-19 situation, the high–high aggregation of RAs has gradually shifted from the commercial circle of Weiyang District back to the cultural and tourism center of the Beilin District. Additionally, the standard deviation ellipse method was used to analyze the center of gravity distribution patterns, which showed a shift from northwest to southeast for both RAs and TFs. The turning angle and area of the standard deviation ellipse have decreased, reflecting the increasing aggregation of RAs and TFs in the main urban area of Xi'an.

In conclusion, this research analyzed the spatiotemporal patterns of RAs and TFs in Xi'an's main urban area over the past decade, revealing their evolution, spatial layout, and center of gravity distribution patterns. These findings have significant implications for urban planning and development in the region, particularly in the context of post-COVID-19 recovery. However, this study still has some limitations, as it has neglected the influence of various factors on the results, including natural factors such as altitude, terrain, and climate, as well as socio-economic factors such as industry policies, market demand, and economic benefits. The research conducted may impact the comprehensiveness and accuracy of the study. Future research should consider incorporating multiple data sources and obtaining information from a wider variety of official sources to enrich and support the study. Finally, conducting comparative studies from different research scales (administrative boundaries, grids, and TAZs) is an expandable research topic.

6. Suggestions

Based on the research conclusions of this paper, suggestions are made for the following four aspects:

(1) Strengthen the relationship between research findings and urban planning. Use the insights gained from the spatial analysis of RATFs to inform urban planning decisions. This includes adjusting the distribution of employment opportunities and residential areas, ensuring that both are well served by transportation networks and promoting mixed-use development to reduce the separation of work and residence.

(2) Improve access to essential facilities in RAs. Based on the identified disparities in facility configuration, prioritize investments in transportation and public infrastructure in underserved areas. This includes improving access to public transit stations, commercial areas, and medical facilities. Additionally, optimize the transport network to enhance the quality and coverage of public transport near residential areas.

(3) Promote diverse and adaptable residential planning. Acknowledge the needs and characteristics of different demographic groups, such as the elderly, disabled, and families, when planning RAs. This should include providing suitable housing options, ensuring adequate infrastructure, and creating a supportive community environment.

(4) Optimize urban spatial layout (e.g., for TFs). Plan the layout and spatial connections of housing and TFs to promote coordinated development and avoid over-concentration in a single area. Enhance road capacity by improving road layout and increasing channel width, and adopt a traffic-oriented development approach, which considers traffic demand in urban planning and aligns transport development with urban planning goals.

Author Contributions: Data curation, C.G.; formal analysis, X.L. and C.G.; methodology, X.L.; validation, C.G.; visualization, X.L.; writing—original draft, X.L. and C.G.; writing—review and editing, C.G. All authors have read and agreed to the published version of the manuscript.

Data Availability Statement: A sample dataset is available upon request to the corresponding author.

Conflicts of Interest: The authors declare no conflict of interest.

References

1. Jiang, Y.; Zhang, Y.; Liu, Y.; Huang, Z. A Review of Urban Vitality Research in the Chinese World. *Trans. Urban Data Sci. Technol.* **2023**, 275412312311547. [CrossRef]
2. Ewing, R.; Cervero, R. Travel and the Built Environment. *J. Am. Plan. Assoc.* **2010**, *76*, 265–294. [CrossRef]
3. Harvey, D. *Social Justice and the City*; University of Georgia Press: Athens, GA, USA, 2010; Volume 1.
4. Lynch, K. *Reconsidering the Image of the City*; Springer: Berlin/Heidelberg, Germany, 1984.
5. Cervero, R.; Kockelman, K. Travel Demand and the 3Ds: Density, Diversity, and Design. *Transp. Res. Part D Transp. Environ.* **1997**, *2*, 199–219. [CrossRef]
6. Bai, X.; Roberts, B.; Chen, J. Urban Sustainability Experiments in Asia: Patterns and Pathways. *Environ. Sci. Policy* **2010**, *13*, 312–325. [CrossRef]
7. Zhang, X.; Pan, J. Spatiotemporal Pattern and Driving Factors of Urban Sprawl in China. *Land* **2021**, *10*, 1275. [CrossRef]
8. Zhou, Z.; Yu, J.; Guo, Z.; Liu, Y. Visual Exploration of Urban Functions via Spatio-Temporal Taxi OD Data. *J. Vis. Lang. Comput.* **2018**, *48*, 169–177. [CrossRef]
9. Miao, R.; Wang, Y.; Li, S. Analyzing Urban Spatial Patterns and Functional Zones Using Sina Weibo POI Data: A Case Study of Beijing. *Sustainability* **2021**, *13*, 647. [CrossRef]
10. Formánek, T.; Sokol, O. Location Effects: Geo-Spatial and Socio-Demographic Determinants of Sales Dynamics in Brick-and-Mortar Retail Stores. *J. Retail. Consum. Serv.* **2022**, *66*, 102902. [CrossRef]
11. Batty, M. Big Data, Smart Cities and City Planning. *Dialogues Hum. Geogr.* **2013**, *3*, 274–279. [CrossRef]
12. Liu, X.; Long, Y. Automated Identification and Characterization of Parcels with OpenStreetMap and Points of Interest. *Environ. Plan. B Plan. Des.* **2016**, *43*, 341–360. [CrossRef]
13. Song, J.; Lin, T.; Li, X.; Prishchepov, A.V. Mapping Urban Functional Zones by Integrating Very High Spatial Resolution Remote Sensing Imagery and Points of Interest: A Case Study of Xiamen, China. *Remote Sens.* **2018**, *10*, 1737. [CrossRef]
14. Zhai, W.; Bai, X.; Shi, Y.; Han, Y.; Peng, Z.-R.; Gu, C. Beyond Word2vec: An Approach for Urban Functional Region Extraction and Identification by Combining Place2vec and POIs. *Comput. Environ. Urban Syst.* **2019**, *74*, 1–12. [CrossRef]
15. Wang, Y.; Gu, Y.; Dou, M.; Qiao, M. Using Spatial Semantics and Interactions to Identify Urban Functional Regions. *ISPRS Int. J. Geo-Inf.* **2018**, *7*, 130. [CrossRef]
16. Gao, S.; Janowicz, K.; Couclelis, H. Extracting Urban Functional Regions from Points of Interest and Human Activities on Location-Based Social Networks. *Trans. GIS* **2017**, *21*, 446–467. [CrossRef]
17. Yue, Y.; Zhuang, Y.; Yeh, A.G.; Xie, J.-Y.; Ma, C.-L.; Li, Q.-Q. Measurements of POI-Based Mixed Use and Their Relationships with Neighbourhood Vibrancy. *Int. J. Geogr. Inf. Sci.* **2017**, *31*, 658–675. [CrossRef]
18. Shi, K.; Chang, Z.; Chen, Z.; Wu, J.; Yu, B. Identifying and Evaluating Poverty Using Multisource Remote Sensing and Point of Interest (POI) Data: A Case Study of Chongqing, China. *J. Clean. Prod.* **2020**, *255*, 120245. [CrossRef]
19. Wu, C.; Ye, X.; Ren, F.; Du, Q. Check-in Behaviour and Spatio-Temporal Vibrancy: An Exploratory Analysis in Shenzhen, China. *Cities* **2018**, *77*, 104–116. [CrossRef]
20. Liu, X.; He, J.; Yao, Y.; Zhang, J.; Liang, H.; Wang, H.; Hong, Y. Classifying Urban Land Use by Integrating Remote Sensing and Social Media Data. *Int. J. Geogr. Inf. Sci.* **2017**, *31*, 1675–1696. [CrossRef]
21. Louail, T.; Lenormand, M.; Cantu Ros, O.G.; Picornell, M.; Herranz, R.; Frias-Martinez, E.; Ramasco, J.J.; Barthelemy, M. From Mobile Phone Data to the Spatial Structure of Cities. *Sci. Rep.* **2014**, *4*, 5276. [CrossRef]
22. Zheng, F.; Hu, Y. Assessing Temporal-Spatial Land Use Simulation Effects with CLUE-S and Markov-CA Models in Beijing. *Environ. Sci. Pollut. Res.* **2018**, *25*, 32231–32245. [CrossRef]
23. Novack, T.; Vorbeck, L.; Lorei, H.; Zipf, A. Towards Detecting Building Facades with Graffiti Artwork Based on Street View Images. *ISPRS Int. J. Geo-Inf.* **2020**, *9*, 98. [CrossRef]
24. Liu, C.; Chen, L.; Yuan, Q.; Wu, H.; Huang, W. Revealing Dynamic Spatial Structures of Urban Mobility Networks and the Underlying Evolutionary Patterns. *ISPRS Int. J. Geo-Inf.* **2022**, *11*, 237. [CrossRef]
25. Ahvenniemi, H.; Huovila, A.; Pinto-Seppä, I.; Airaksinen, M. What Are the Differences between Sustainable and Smart Cities? *Cities* **2017**, *60*, 234–245. [CrossRef]
26. Chen, Y.; Yu, B.; Shu, B.; Yang, L.; Wang, R. Exploring the Spatiotemporal Patterns and Correlates of Urban Vitality: Temporal and Spatial Heterogeneity. *Sustain. Cities Soc.* **2023**, *91*, 104440. [CrossRef]
27. Zhu, H.; Zhang, K.; Wang, C.; Jia, L.; Song, S. The Impact of Road Functions on Road Congestions Based on POI Clustering: An Empirical Analysis in Xi'an, China. *J. Adv. Transp.* **2023**, *2023*, 6144048. [CrossRef]
28. Botta, F.; Gutiérrez-Roig, M. Modelling Urban Vibrancy with Mobile Phone and OpenStreetMap Data. *PLoS ONE* **2021**, *16*, e0252015. [CrossRef]
29. Yang, X.; Fang, Z.; Yin, L.; Li, J.; Lu, S.; Zhao, Z. Revealing the Relationship of Human Convergence–Divergence Patterns and Land Use: A Case Study on Shenzhen City, China. *Cities* **2019**, *95*, 102384. [CrossRef]
30. Duong, T. Ks: Kernel Density Estimation and Kernel Discriminant Analysis for Multivariate Data in R. *J. Stat. Softw.* **2007**, *21*, 1–16. [CrossRef]

31. Song, Y.; Wang, J.; Ge, Y.; Xu, C. An Optimal Parameters-Based Geographical Detector Model Enhances Geographic Characteristics of Explanatory Variables for Spatial Heterogeneity Analysis: Cases with Different Types of Spatial Data. *GISci. Remote Sens.* **2020**, *57*, 593–610. [CrossRef]
32. Yu, W.; Ai, T.; Shao, S. The Analysis and Delimitation of Central Business District Using Network Kernel Density Estimation. *J. Transp. Geogr.* **2015**, *45*, 32–47. [CrossRef]
33. Zhang, X.; Yao, J.; Sila-Nowicka, K. Exploring Spatiotemporal Dynamics of Urban Fires: A Case of Nanjing, China. *ISPRS Int. J. Geo-Inf.* **2018**, *7*, 7. [CrossRef]
34. Zhao, Y.; Wu, Q.; Wei, P.; Zhao, H.; Zhang, X.; Pang, C. Explore the Mitigation Mechanism of Urban Thermal Environment by Integrating Geographic Detector and Standard Deviation Ellipse (SDE). *Remote Sens.* **2022**, *14*, 3411. [CrossRef]
35. Lin, Y.; Hu, X.; Lin, M.; Qiu, R.; Lin, J.; Li, B. Spatial Paradigms in Road Networks and Their Delimitation of Urban Boundaries Based on KDE. *ISPRS Int. J. Geo-Inf.* **2020**, *9*, 204. [CrossRef]
36. Zhang, X.; Sun, Y.; Chan, T.; Huang, Y.; Zheng, A.; Liu, Z. Exploring Impact of Surrounding Service Facilities on Urban Vibrancy Using Tencent Location-Aware Data: A Case of Guangzhou. *Sustainability* **2021**, *13*, 444. [CrossRef]